High-resolution autofocus techniques for SAR imaging based on fractional lower-order statistics

P.Tsakalides and C.L.Nikias

Abstract: The authors address the autofocusing problem in synthetic aperture radar imagery by introducing techniques that achieve robust image formation in the presence of severe heavy-tailed clutter and noise. Current state-of-the-art methods are extended, which are based on second-order moment theory, by employing fractional lower-order statistics (FLOS) of the phase-history data. The introduced FLOS-based methods perform a nonlinear transformation of the radar measurements, can mitigate the effects of impulsive additive clutter, and include the conventional algorithms as special cases. The benefits of the proposed approach are quantified by means of simulations, and the new FLOS-based methods are compared to current state-of-the-art processing with real synthetic aperture radar imagery data.

1 Introduction

In many coherent radar signal processing applications it is assumed that certain relative motions exist between the radar system and its target [1]. For example, in strip-mapping synthetic aperture radar (SAR) the radar's aircraft platform is assumed to travel in a perfectly straight line at constant velocity; or in turntable inverse SAR (ISAR) the target is assumed to rotate at a constant angular rate. In practice, the motion between the radar and the target does not meet this ideal. Even under the best circumstances, turbulence and vibration will cause the aircraft's flight path to deviate arbitrarily from the assumed coordinates. As a result, motion compensation mechanisms are required to alleviate the effects of the radar's deviation from the assumed ideal path.

Motion compensation of SAR data is critical to the achievement of optimal resolution in SAR imagery. More specifically, increasing the system resolution rapidly increases motion compensation accuracy requirements. As pointed out in [2], uncompensated motion results in serious image defocusing caused by the presence of quadratic and higher-order phase errors. Autofocus techniques use the SAR data itself to estimate and remove the phase errors from the same data. Accurate extraction of motion-induced phase errors from SAR measurements is dependent on the specific scene imaged and on the particular autofocus algorithm used. Many existing autofocus algorithms assume that the phase errors are space-invariant in azimuth and apply the same correction vector to all scatterers in the image. Most importantly, their underlying mathematical methodology is entirely based on the Fourier transform and on the second-order statistics of along-azimuth data.

Several distinct approaches to SAR system autofocusing have been proposed [2]: mapdrift (MD), multiple aperture mapdrift (MAM), phase difference (PD), the original phase gradient autofocus (PGA) and the maximum-likelihood-based PGA (PGA-ML). These methods may be divided into parametric, sub-aperture (MD, MAM, PD) and non-parametric, full-aperture (PGA, PGA-ML) classes. They work in an iterative way, and they assume space-invariant phase errors over sub-aperture blocks of different sizes. Usually, they are applied relative only to one-dimensional phase errors, because azimuth phase errors are the primary SAR error concern. Of course, the techniques apply equally to range phase errors as well. Each technique has its own advantages and limitations in terms of performance, complexity and ease of implementation.

The mapdrift (MD) method divides the aperture into two non-overlapping sub-apertures and then estimates the Doppler shift (DS) between the two along-azimuth signals by a cross-correlation operation, i.e. by employing second-order statistics. The actual location of the correlation peak is used to estimate the phase correction to apply to the data, which can then be refocused [3]. An average DS estimate is obtained using approximately 5% of the range bins containing most of the energy. The multiple aperture mapdrift (MAM) technique is an extension of the MD algorithm that estimates higher-order phase errors by dividing the aperture into more than two sub-apertures [4]. In general, N sub-apertures are adequate to estimate the coefficients of an Nth-order polynomial error. Both MD and MAM are parametric methods, i.e. they assume that the phase error is described by a polynomial. As a consequence, the methods are limited to estimating low-order phase error functions, because the sub-apertures required to estimate high-order polynomial coefficients become so small that the correlation measures are inaccurate.

IEE Proceedings online no. 20010457

DOI: 10.1049/ip-rsn:20010457

Paper first received 17th September 1999 and in final revised form 26th January 2001

P. Tsakalides is with the Signal Processing Systems Group, Department of Electrical and Computer Engineering, University of Patras, 261 10 Rio, Greece

C.L. Nikias is with the Integrated Media Systems Center, Department of Electrical Engineering, University of Southern California, CA 90089-2561, USA

The phase difference (PD) technique divides the aperture into two sub-apertures and estimates the DS parameter using a second-order ambiguity function [5]. The PD algorithm achieves results comparable to MD with fewer computations, because it is able to generate an accurate phase-error measurement without first cancelling the major portion of the error being measured, thus eliminating the need for an iterative computation.

The phase gradient autofocus method (PGA) is recognised today as a powerful, full-aperture, non-parametric technique that allows precise estimation and compensation of higher-order phase errors. The method is based on the redundancy of the available measurements, and on the fact that the received data over the whole aperture and the complex image form a Fourier transform pair. The PGA kernel, originally introduced in [6], estimates the entire phase error function by locating the peak amplitude function within each azimuth over all the compressed range bins and by computing its first derivative using the derivative property of the Fourier transform. The integration of the phase gradient provides the phase error function estimate. Then, the phase estimates are averaged over many range bins in a weighted least-squares sense.

The original PGA kernel was shown to be sensitive to the presence of clutter/noise and to suffer from aliasing effects due to the derivative computation with the Fourier transform. To address this problem, a maximum likelihood version of the PGA (PGA-MLG) was introduced, based on formal optimal estimation theory [7, 8]. PGA-MLG achieves the Cramér–Rao lower bound and may be tuned to use an arbitrary number of azimuth pixels to estimate the phase error.

Existing autofocus techniques for estimating Doppler shifts and/or pulse delays from echoed signals are based on second-order statistics and cross-correlation operations. A serious problem arises when the autofocusing has to be performed in the presence of severe clutter, noise and other interfering sources such as jammers. In such environments, signal processing systems based on second-order cross-correlation techniques exhibit significant performance degradation [9, 10]. This paper shows that second-order based autofocus methods operating in severe clutter backgrounds provide Doppler shifts and/or pulse delay estimates that may be severely biased. In the presence of severe clutter and interference, the frequency shifts of two adjacent azimuth spectra can be estimated more accurately by methods that have the inherent capability of enhancing output signal-to-interference/clutter ratio and of being robust in the presence of mismatches in the assumed conditions of clutter and interference.

In this paper, we extend current state-of-the-art methods by employing fractional lower-order statistics (FLOS) of the phase-history data. The introduced FLOS-based methods can mitigate the effects of heavy-tailed additive clutter in the measurements and achieve high-resolution SAR image formation. The new algorithms are applicable to SAR processing problems where the existing clutter can be modelled as an alpha-stable process.

2 Alpha-stable models and their properties

It is recognised that effective phase error correction of SAR imagery in the presence of background clutter can be achieved only on the basis of appropriate statistical modelling and high target-to-clutter ratios [7]. The probabilistic models currently employed are based almost exclusively on the Gaussian or other families of distributions, such as the K, the Weibull and the log-normal, which possess exponential tails [11–13]. In many real life applications, these distributions fail to provide reasonable agreement between the theoretical and the experimentally observed statistics, especially in the case of heavy-tailed clutter [14, 15]. Therefore, SAR autofocusing signal processing design cannot be reliably based exclusively on exponentially tailed models but rather on families of possibly heavy-tailed distributions.

The alpha-stable statistical models and their corresponding fractional lower-order statistics (FLOS) comprise a newly emerging and rapidly expanding signal processing methodology with a potential for many radar signal processing applications [9]. A complex random variable $X=X_1+jX_2$ is symmetrically α-stable (SαS) if X_1 and X_2 are jointly SαS and then its characteristic function is written as

$$\varphi(\omega) = E\{\exp[j\Re(\omega X^*)]\} = E\{\exp[j(\omega_1 X_1 + \omega_2 X_2)]\} = \exp\left[-\int_{S_2} |\omega_1 x_1 + \omega_2 x_2|^\alpha \, d\Gamma_{X_1,X_2}(x_1, x_2)\right] \quad (1)$$

where $\omega=\omega_1+j\omega_2$, $\Re[\cdot]$ is the real-part operator, and Γ_{X_1,X_2} is a symmetric measure on the unit sphere S_2, called the 'spectral measure' of the random variable X. The characteristic exponent α is restricted to the values $0<\alpha\leq 2$ and it determines the shape of the distribution. The smaller the characteristic exponent α, the heavier the tails of the density, see Fig. 1.

A complex random variable $X=X_1+jX_2$ is isotropic if, and only if, (X_1, X_2) has a uniform spectral measure. In this case, the characteristic function of X can be written as

$$\varphi(\omega) = E\{\exp(j\Re[\omega X^*])\} = \exp(-\gamma\,|\omega|^\alpha) \quad (2)$$

where γ ($\gamma>0$) is the dispersion of the distribution. The dispersion plays a role analogous to the role that the variance plays for second-order processes. Namely, it determines the spread of the probability density function around the origin.

Alpha-stable densities obey two important properties, which justify their role in data modelling:

- *The stability property*: This states that the weighted sum of independent alpha-stable random variables is again stable with the same characteristic exponent alpha.
- *The generalised central limit theorem (GCLT)*: This

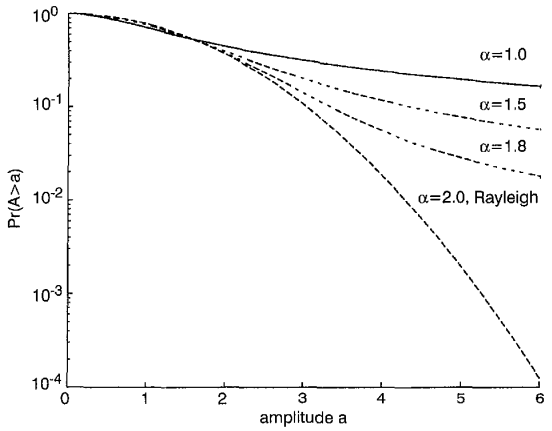

Fig. 1 *Symmetric alpha-stable amplitude probability density (APD) functions (Pr(A > a))*

Dispersion is $\gamma=1$ and characteristic exponent is $\alpha=1.0$, 1.5, 1.8, and $\alpha=2.0$ (Rayleigh)

states that stable models provide the only possible limiting distributions for the sum of independent, identically distributed random variables.

In other words, GCLT says that if the observed randomness is the result of many cumulative effects (as is the case in clutter formation due to reflections from many scatterers), and these effects follow a heavy-tailed distribution, then a stable model may be appropriate. In addition, unlike the Gaussian distribution which is symmetric about its mean, stable distributions may also be asymmetric, i.e. they admit skewness. Therefore, in certain applications where a heavy-tailed and asymmetric model is called for, the stable model is a viable alternative to the Gaussian distribution.

Fig. 2 shows indicative results on the modelling of the amplitude statistics of real radar imagery data (cf. Fig. 8, Section 4.2) by means of symmetric alpha-stable (SαS) distributions. The data were provided by Dr. D. E. Wahl of Sandia National Laboratories in New Mexico, USA, and they are used in Section 4.2 to test the proposed PGA-FLOS autofocus method. A comparison is made to determine how close the Gaussian, SαS, Weibull and log-normal distributions approximate the empirical amplitude probability density corresponding to the actual radar time series. The estimation of the parameters of the stable distribution from the actual radar data was achieved by using the maximum-likelihood method described by Nolan in [16], which gives reliable estimates and provides the most tight confidence intervals. For the particular data used here, the characteristic exponent of the SαS distribution which best fits the data was calculated to be approximately $\alpha = 1.5094$, with an associated 95% confidence interval equal to 0.01. Fig. 2 shows that the SαS distribution provides a better fit to both the mode and the tails of the empirical density of the actual data, than the Gaussian, Weibull and the log-normal distributions. This is due to the fact that stable laws have inverse power (i.e. algebraic) tails, which decay much slower than the exponential tails of the Gaussian, Weibull and log-normal laws.

Indeed, let X be a non-Gaussian SαS random variable. Then, as $x \to \infty$

$$P(|X| > x) \sim c_\alpha x^{-\alpha} \tag{3}$$

where $c_\alpha = \Gamma(\alpha)[\sin(\pi\alpha/2)]/\pi$, $\Gamma(\cdot)$ is the Gamma function, and the statement '$h(x) \sim g(x)$ as $x \to \infty$' means that

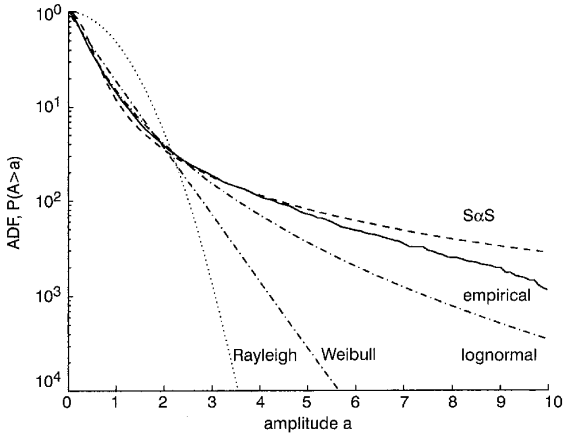

Fig. 2 *Statistical modelling of the SAR data shown in Fig. 8a: amplitude probability density curves*

Distribution parameters: Rayleigh with parameter $\sigma = 0.83$; SαS with $\alpha = 1.51$, $\gamma = 0.13$; Weibull with scale $\eta = 1.68$ and shape $\sigma = 0.98$; log-normal with $\mu = -1.02$ and $\sigma = 0.98$

$\lim_{x\to\infty} h(x)/g(x) = 1$. Hence, the tail probabilities are asymptotically power laws. Fig. 1 shows the tail behaviour of several SαS densities including the Cauchy and the Gaussian. We should note that because expr. 3 gives exactly the tail probability of the Pareto distribution, the term 'stable Paretian laws' is used to distinguish between the fast decay of the Gaussian law and the Pareto-like tail behaviour when $\alpha < 2$.

Because of this algebraic tail behaviour, only moments of order less than α exist for the non-Gaussian alpha-stable family members. In the theory of second-order processes, the concept of covariance plays an important role in problems of linear prediction, filtering and smoothing. Since alpha-stable processes do not possess finite pth order moments for $p \geq \alpha$, covariances do not exist on the space of non-Gaussian alpha-stable random variables. Instead, a quantity called covariation plays an analogous role in statistical signal processing problems involving stable processes, to the role played by the covariance in the case of second-order processes. The covariation of X and Y is defined by

$$[X, Y]_\alpha = \frac{E\{XY^{\langle p-1\rangle}\}}{E\{|Y|^p\}}\gamma_Y \tag{4}$$

for every $1 \leq p < \alpha$ and where we use throughout the convention

$$Y^{\langle\beta\rangle} = |Y|^{\beta-1}\, Y^* \tag{5}$$

The covariation of the jointly SαS random variables X and Y is not generally symmetric and has the following properties [17]:

P1: If X_1, X_2 and Y are jointly SαS, then

$$[aX_1 + bX_2, Y]_\alpha = a[X_1, Y]_\alpha + b[X_2, Y]_\alpha \tag{6}$$

for any complex constants a and b.

P2: If Y_1 and Y_2 are independent and Y_1, Y_2, and X are jointly SαS, then

$$[aX, bY_1 + cY_2]_\alpha = ab^{\langle\alpha-1\rangle}[X, Y_1]_\alpha + ac^{\langle\alpha-1\rangle}[X, Y_2]_\alpha \tag{7}$$

where a, b and c are arbitrary complex constants and the signed nonlinearity is defined in eqn. 5.

P3: If X and Y are independent SαS, then $[X, Y]_\alpha = 0$.

We extend the notion of covariation by defining the fractional lower-order statistics (FLOS) of two arbitrary and possibly heavy-tailed random variables x, y of the zero location parameter and finite pth-order moment

$$E[|x|^p] > \infty, \qquad E[|y|^p] > \infty \tag{8}$$

for some possibly fractional p, $0 < p \leq 2$. The FLOS-based correlation function is then defined as

$$\langle x, y\rangle_{p_1,p_2} = E[x^{\langle p_1\rangle}\, y^{*\langle p_2\rangle}] \tag{9}$$

When the random variables x and y are SαS with characteristic exponent α, the parameters p_1 and p_2 should be chosen to satisfy $p_1 + p_2 < \alpha$ so that the expression in eqn. 9 is finite. Choosing $p_1 = p_2 < \alpha/2$ satisfies this condition. Clearly, when $p_1 = p_2 = 1$ the above FLOS definition reduces to the usual correlation function between x and y.

Compared with existing statistical models for noise, clutter and interference, signal processing algorithms based on alpha-stable models for detection, parameter estimation and array processing demonstrate robustness even in the presence of mismatches in the assumed conditions of clutter and interference [9, 10, 18]. In addition, the

use of fractional lower-order statistics and covariations is indeed simple to understand and implement in real-time processing scenarios.

3 Robust autofocus methods based on FLOS

In the following Sections, we introduce three new autofocus methods based on FLOS, namely the mapdrift (MD-FLOS), phase difference (PD-FLOS) and phase gradient algorithm (PGA-FLOS).

3.1 Mapdrift autofocus method based on FLOS (MD-FLOS)

Assuming that T_a is the duration of the synthetic aperture and a is the quadratic phase error coefficient, the two sub-aperture 'along-azimuth' range-compressed signals are given by

$$x(t) = s(t)\exp\{-j\Delta\omega t\} + \omega_1(t)$$
$$y(t) = s(t)\exp\{+j\Delta\omega t\} + \omega_2(t) \quad (10)$$

where $-T_a/4 \leq t \leq T_a/4$, $\Delta\omega = aT_a/2$, $s(t)$ is the error-free signal history and $\omega_1(t)$ and $\omega_2(t)$ are the noise/clutter components. The goal is to estimate $\Delta\omega$, and thus the parameter $a = 2\Delta\omega/T_a$, from the noisy measurements $x(t)$ and $y(t)$.

When the two noise/clutter components are assumed to have a heavy-tailed distribution, solving the problem in the fractional lower-order domain results in improved phase-error estimates because FLOS metrics have been shown to suppress impulsive noise [18]. The idea behind the MD-FLOS algorithm is to use the FLOS of the data, i.e. to cross-correlate nonlinear transformations of the left and right sub-aperture signals. The proposed method proceeds in the following steps:

Step 1: Transform each sub-aperture $x(t)$ and $y(t)$ according to

$$x_{p_1}(t) = x^{\langle p_1\rangle}(t) = |x(t)|^{p_1-1}x^*(t)$$
$$y_{p_2}(t) = y^{\langle p_2\rangle}(t) = |y(t)|^{p_2-1}y^*(t)$$
$$0 < p_1, p_2 \leq \alpha/2 \quad (11)$$

Note that the nonlinear operation described in eqns. 11 preserves the phase information of the measurements and compresses their amplitude in such a way as to bound statistical entities that otherwise would be infinite in the presence of SαS clutter and noise.

Step 2: Fourier transform $x_{p_1}(t)$ and $y_{p_2}(t)$ into the image domain to get $X_{p_1}(\omega)$, $Y_{p_2}(\omega)$.

Step 3: Estimate the shift a by measuring the peak location of the cross-correlation of the two intensity images.

Note that when $p_1 = p_2 = 1.0$, we get the conventional mapdrift method as a special case.

3.2 Phase difference autofocus method based on FLOS (PD-FLOS)

The conventional PD algorithm is based on the second-order ambiguity function:

$$A_{xy}^{(2)}(\omega, \tau) = \int_{-T_a/4}^{T_a/4} x(t)y^*(t+\tau)e^{-j\omega t}dt \quad (12)$$

The values (ω, τ) that maximise $|A_{xy}^{(2)}(\omega, \tau)|$ are the estimates of the Doppler shift (DS) and pulse delay, respectively. Since we are only interested in the DS estimate, the slice $A_{xy}^{(2)}(\omega, \tau = 0)$ is computed from the data.

In alpha-stable noise environments, the definition of the ambiguity function in eqn. 12 was extended to the so-called fractional lower-order ambiguity function (FLOAF), which is able to give more accurate DS estimates than the second-order ambiguity function in the presence of impulsive clutter [19]. Based on this definition, we introduce the use of the FLOAF of the left and right sub-aperture signals. The resulting PD-FLOS algorithm consists of the following steps:

Step 1: Transform each sub-aperture $x(t)$ and $y(t)$ according to eqns. 11.

Step 2: Form the product $z(t) = y_{p_2}(t)x_{p_1}^*(t)$; $-T_a/4 \leq t \leq T_a/4$.

Step 3: Take the Fourier transform of $z(t)$, thus producing a cross-correlation of the transformed complex images from each sub-aperture:

$$A_{xy}^{(p_1,p_2)}(\omega) = \int_{-T_a/4}^{T_a/4} z(t)e^{-j\omega t}dt \quad (13)$$

Step 4: Estimate the shift a by measuring the peak location of $|A_{xy}^{(p_1,p_2)}(\omega)|$.

Note that when $p_1 = p_2 = 1.0$, we get the second-order phase-difference method.

3.3 FLOS-based phase-gradient autofocus method (PGA-FLOS)

This Section describes the phase-gradient autofocus (PGA) algorithm based on FLOS for automatic estimation and correction of high-order phase errors in spotlight-mode SAR imagery. The PGA-FLOS algorithm, unlike the MD-FLOS and PD-FLOS ones, is not model-based, i.e. implementation does not require a polynomial expression for the phase error function. In addition, it takes advantage of the redundancy of the phase error function by averaging across many range cells.

The PGA algorithm, as applied by Wahl *et al.* in [8], consists of several critical steps that include: (i) centre (circular) shifting, (ii) windowing, (iii) phase difference estimation and (iv) iterative correction. These algorithmic steps are shown in the flow diagram of Fig. 3. The centre shifting and windowing operations are common to all PGA versions [7]. Firstly, PGA selects the strongest target on each range line and circularly shifts it to the scene centre. This operation preserves the effects of the phase error on the selected target, while simultaneously removing any linear phase component associated with the target. The shifting operation creates a new image where all the targets are aligned and stacked in the centre of the scene.

The intent of the windowing step is to preserve the phase error information contained in the centre shifted targets, while at the same time rejecting information from all other surrounding clutter and targets that cannot contribute to phase-error estimation. This step in effect allows the algorithm to proceed by using data having the highest signal-to-noise ratio. Width selection strategies are described in [8]. After windowing, a Fourier transform is applied in the cross-range dimension on each range line to go to the range-compressed domain.

The phase error estimation kernel is the heart of the PGA method. Consider samples of range-compressed data for which there are N range lines and M aperture positions, so that a total of $M \times N$ samples are used. In the range-

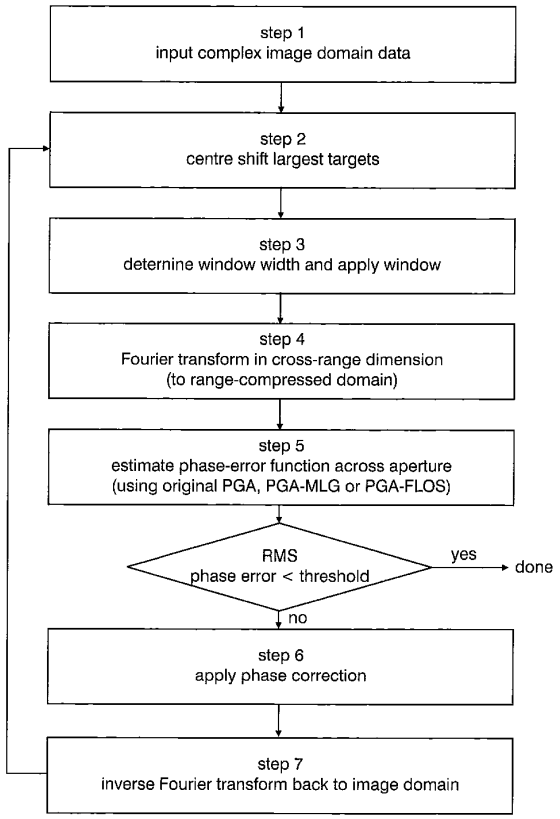

Fig. 3 *Flow diagram of the phase gradient autofocus (PGA) algorithm*

compressed domain, the phase errors are modelled such that between the lth and first aperture positions there exists a phase difference ψ_l that is constant across all range lines. The model for the centre-shifted, windowed and transformed data at the kth range bin is then taken to be

$$\begin{aligned} g_{k1} &= a_k + n_{k1} \\ g_{k2} &= a_k e^{j\psi_2} + n_{k2} \\ &\vdots = \vdots \\ g_{kM} &= a_k e^{j\psi_M} + n_{kM} \end{aligned} \tag{14}$$

where $k = 1, \ldots, N$ and g_{kl} represents the sample aperture position l on the kth range bin. The phase at the first aperture position is arbitrarily assigned the value of zero.

A direct approach to the phase-estimation problem is to use all $N \times M$ data points to derive a maximum-likelihood (ML) estimate of ψ_i. Jakowatz and Wahl introduced an eigenvector method for ML phase error compensation with Gaussian data, which uses all M pulse vectors in the range-compressed domain to simultaneously estimate $M-1$ phase values across the aperture [7]. Their solution involves the eigenvector corresponding to the largest eigenvalue of the data sample covariance matrix. They showed that the general PGA-MLG technique for the special case of $M=2$ collapses to an estimator that uses data on two adjacent pulses at a time to estimate the phase difference between them. These differences may then be integrated to obtain an estimate for the entire ψ_i. Although the adjacent-pulse version in general requires more iterations than are needed when larger values of M are employed, its simplicity makes it the algorithm of choice.

In our model, the real and imaginary (I and Q) components of the complex reflectivity of a point target on each range line are treated as symmetrically alpha-stable (SαS) random variables. In addition, the clutter reflectivity I and Q values are also modelled as independent SαS random variables. All clutter and target components are mutually independent across all values of the range and cross range. The introduced PGA-FLOS algorithm uses adjacent pulse pairs only. It is based on the covariation of the sample at the ith aperture position, g_{ki}, with the sample at the jth aperture position, g_{kj}.

Considering the covariation of g_{ki} with g_{kj} and by using properties $P1$ to $P3$ we get:

$$\begin{aligned} [g_{ki}, g_{kj}]_\alpha &= [a_k e^{j\psi_i} + n_{ki}, a_k e^{j\psi_j} + n_{kj}]_\alpha \\ [\text{using } P1] &= e^{j\psi_i}[a_k, a_k e^{j\psi_j} + n_{kj}]_\alpha + [n_{ki}, a_k e^{j\psi_j} + n_{kj}]_\alpha \\ [\text{using } P2] &= e^{j\psi_i}(e^{j\psi_j})^{\langle\alpha-1\rangle}[a_k, a_k]_\alpha + e^{j\psi_i}[a_k, n_{kj}]_\alpha \\ &\quad + (e^{j\psi_j})^{\langle\alpha-1\rangle}[n_{ki}, a_k]_\alpha + [n_{ki}, n_{kj}]_\alpha \\ [a_k \perp n_{kl}] &= \gamma_{a_k} e^{j(\psi_i - \psi_j)} + \delta_{ij}\gamma_{n_k} \end{aligned} \tag{15}$$

where γ_{a_k} is the dispersion of a_k, γ_{n_k} is the clutter dispersion of n_k and δ_{ij} is the Kronecker delta function (1 when $i=j$, 0 otherwise). Hence, by using two adjacent-pulse samples (i.e. for $i=m$ and $j=m-1$) and all the available ranges, the covariation-based estimator of the difference of the phase errors, $\Delta\psi_m \equiv \psi_m - \psi_{m-1}$, is

$$\Delta\psi_m^{(PGA\text{-}FLOS)} = \arg\left(\sum_{k=1}^{N}[g_{k,m-1}, g_{k,m}]_\alpha\right) \tag{16}$$

where $\arg(x)$ denotes the principal value of the angle of the complex quantity x, computed in the interval $[-\pi, \pi]$.

In practice, one has to estimate the covariation in eqn. 16 from the two adjacent-pulse samples. One such covariation estimator, based on the fractional lower-order moments (FLOMs) of the stable process, is given by [18]:

$$\widehat{\Delta\psi}_m^{(PGA\text{-}FLOS)} = \arg\left(\sum_{k=1}^{N}(g_{k,m-1})^{\langle p_1\rangle}(g_{k,m}^*)^{\langle p_2\rangle}\right) \tag{17}$$

where $0 \le p_1 < \alpha/2$, $0 \le p_2 < \alpha/2$, and α is the characteristic exponent of the associated stable distribution that best describes the clutter statistics. Analytical and experimental studies on the best choice for the parameters p_1 and p_2 indicate that they should be chosen to lie in the midrange between 0 and $\alpha/2$ [18, 19]. In fact, the proposed PGA-FLOS estimator is a class of FLOS-based phase-estimator kernels parameterised by p_1 and p_2. The different kernels can be used in place of the original PGA kernel within the same algorithmic structure of the PGA method, see Fig. 3. As a result, considerable flexibility can be achieved, a fact that can be used for optimisation purposes in the presence of different clutter operational environments.

Once the estimate for $\widehat{\Delta\psi}_m$ is obtained for all m, the entire aperture phase error is estimated by integrating the $\widehat{\Delta\psi}_m$ values:

$$\hat{\psi}_m = \sum_{l=2}^{m}\widehat{\Delta\psi}_l, \quad \hat{\psi}_1 = 0 \tag{18}$$

Thus, the phase estimation step of the PGA-FLOS algorithm consists of estimating the phase difference for all adjacent pulses by applying eqn. 16 $M-1$ times, and then integrating (summing) the result using eqn. 18.

For comparison purposes, the adjacent-pulse version ($M=2$) of the PGA-MLG method, based on a Gaussian

assumption for the data statistics, employs a second-order cross-correlation to the data:

$$\widehat{\Delta\psi}_m^{(PGA\text{-}MLG)} = \arg\left(\sum_{k=1}^{N} g_{k,m-1}^* g_{km}\right) \tag{19}$$

Comparing eqn. 19 with eqn. 17, we can see that the PGA-MLG is a special member of the family of FLOS-based PGA kernels and it is optimum for Gaussian distributed clutter.

Finally, for purposes of easy reference, the original PGA kernel is given by

$$\widehat{\dot{\Delta\psi}}^{(PGA)}(t) = \frac{\sum_{k=1}^{N} \Im[\dot{g}_k(t) g_k^*(t)]}{\sum_{k=1}^{N} |g_k(t)|} \tag{20}$$

where $\Im[x]$ denotes the imaginary part of a complex number x, $\dot{f}(t)$ denotes the derivative of $f(t)$ with respect to t, and instead of a discrete measurement of the aperture position l, the continuous parameter t is used.

As we can see in eqns. 17, 19 and 20, all methods use only data on adjacent pulses in the range-compressed space to estimate a single value of the phase between the two pulses. These phase differences can then be summed to produce an estimate of the phase error function across the entire aperture. The mathematical forms are different because the estimators were derived with different assumptions for the data statistics and different optimisation criteria.

4 Algorithmic assessment

In this Section, we assess the performance of the MD-FLOS, PD-FLOS and PGA-FLOS algorithms in comparison with the performance of the second-order based MD, PD and PGA algorithms, respectively, using both synthetic and real SAR imagery.

4.1 MD-FLOS and PD-FLOS autofocusing results with synthetic data

To investigate the performance of the FLOS-based MD and PD autofocus techniques, we use the synthetic spotlight SAR image of a plane shown in Fig. 4*a*. The model for the azimuth signal $g(t)$ from a single range bin in the range-compressed phase-history domain is the product of the error-free signal history $s(t)$ and a complex exponential with quadratic phase:

$$g(t) = s(t)e^{jat^2}, \qquad -T_a/2 \le t \le T_a/2 \tag{21}$$

where $a = 70\pi$ is the quadratic phase error coefficient to be estimated and $T_a = [-0.4909, 0.4870]$ is the synthetic aperture duration. The SAR image degraded by this phase error is shown in Fig. 4*b*. Note that radar illumination and near range are from the left side of the image.

First, we focus the degraded SAR image by applying iteratively the MD and MD-FLOS methods. The MD-FLOS method uses the parameters $p_1 = p_2 = 0.2$. At each iteration, the algorithms estimate the quadratic phase error coefficient, a, and apply the estimate to the input signal data. Initially, both the MD and MD-FLOS techniques select 40 range bins containing most of the energy. After

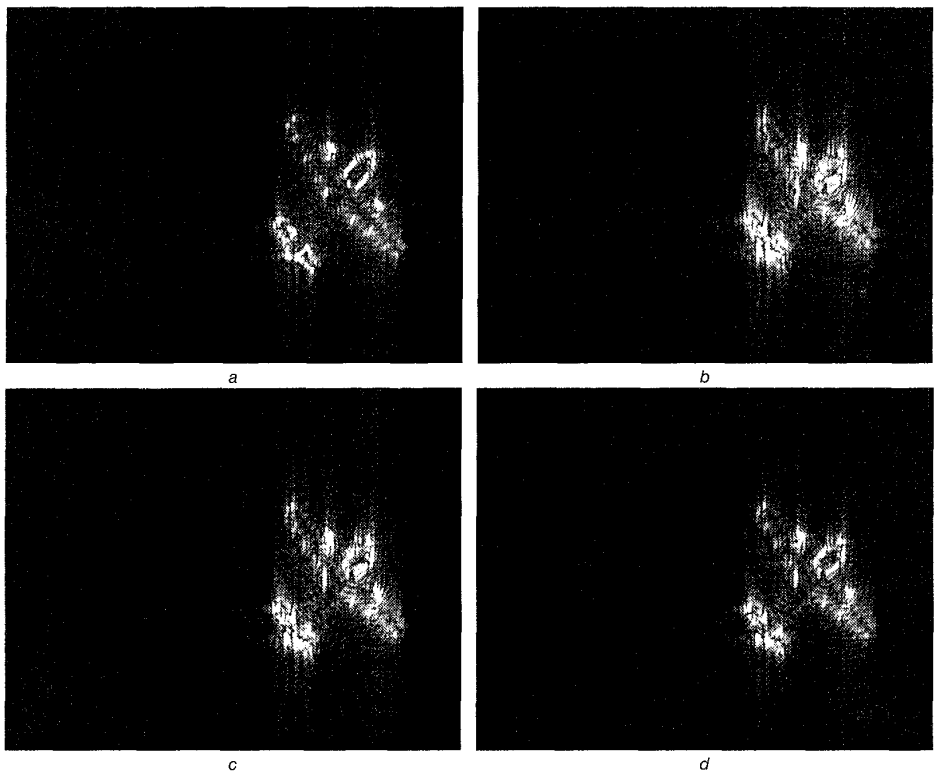

Fig. 4 *Processing of synthetic SAR image of aeroplane*

a Original synthetic SAR image
b SAR image degraded by quadratic phase error
c SAR image focused using second-order mapdrift (MD) method
d SAR image focused using MD-FLOS method with $p_1 = p_2 = 0.2$ after 5 iterations

each iteration, the algorithms discard any range bins with a phase error estimate deviating from the mean estimate by more than one standard deviation. Figs. 4*c* and *d* illustrate the focused SAR images after 5 iterations of MD and MD-FLOS, respectively. It is visually evident that the SAR image obtained by the MD-FLOS method is better focused than the SAR image processed by the MD method. As a quantitative measure of performance, we calculate the root-mean-square (RMS) value of the original phase error subtracted from the phase error estimated by each method. The RMS value of the phase error applied to the original image is 23.70 rad. After 5 iterations, the RMS error associated with MD is 6.97 rad, while the RMS error corresponding to MD-FLOS is 4.72 rad.

We also apply the PD and PD-FLOS algorithms to focus the degraded image. The azimuth signal is divided into two sub-apertures and the PD and PD-FLOS methods estimate the quadratic phase error coefficient at each range bin. Since the use of all range bins improves the signal-to-noise ratio, we average the phase estimates. We use an intensity-weighed average of the individual estimates from each range bin to emphasise phase estimates derived from bins with higher energy. To demonstrate the advantage of the PD-FLOS method over the conventional PD approach in the presence of noise, we degraded the original SAR image both with a quadratic phase error ($a = 100\pi$) and an SαS additive clutter component with $\alpha = 1.75$, which corresponds to the estimated characteristic exponent value of the sea clutter data shown in Fig. 2. The applied effective signal-to-clutter ratio (SCR) is 0 dB [18].

The noisy degraded SAR image is shown in Fig. 5*a*. The RMS value of the applied phase error is 33.85 rad. The focused images obtained by the PD and PD-FLOS algorithms are shown in Figs. 5*b* and 5*c*, *d*, respectively. In this case, we test two versions of the PD-FLOS method: the first employs the parameters $p_1 = p_2 = 0.2$ (Fig. 5*c*), while the second uses $p_1 = p_2 = 0$, i.e. it solely employs the phase information of the measurements and discards their amplitude (Fig. 5*d*). The calculated RMS error associated with PD is 17.36 rad, while the RMS error corresponding to PD-FLOS is 5.78 rad when $p_1 = p_2 = 0.2$ and 6.52 rad when $p_1 = p_2 = 0$.

It is evident in the Figure that, under noisy conditions, the PD method obtains a biased estimate of the phase error and fails to satisfactory focus the SAR image. On the other hand, both PD-FLOS versions estimate the phase error more accurately in the presence of severe noise, and manage to better focus the noisy image. In particular, comparing Figs. 5*c* and *d*, we observe that the PD-FLOS method with parameter values $p_1 = p_2 = 0.2$ achieves better focusing than the PD-FLOS with $p_1 = p_2 = 0$. This implies that the data amplitude should not be laid aside by the estimation process.

4.2 PGA-FLOS autofocusing results with real SAR imagery

In this Section, we study the performance of the second-order and FLOS-based PGA kernels using real radar imagery. The data were provided by Dr. D. E. Wahl of

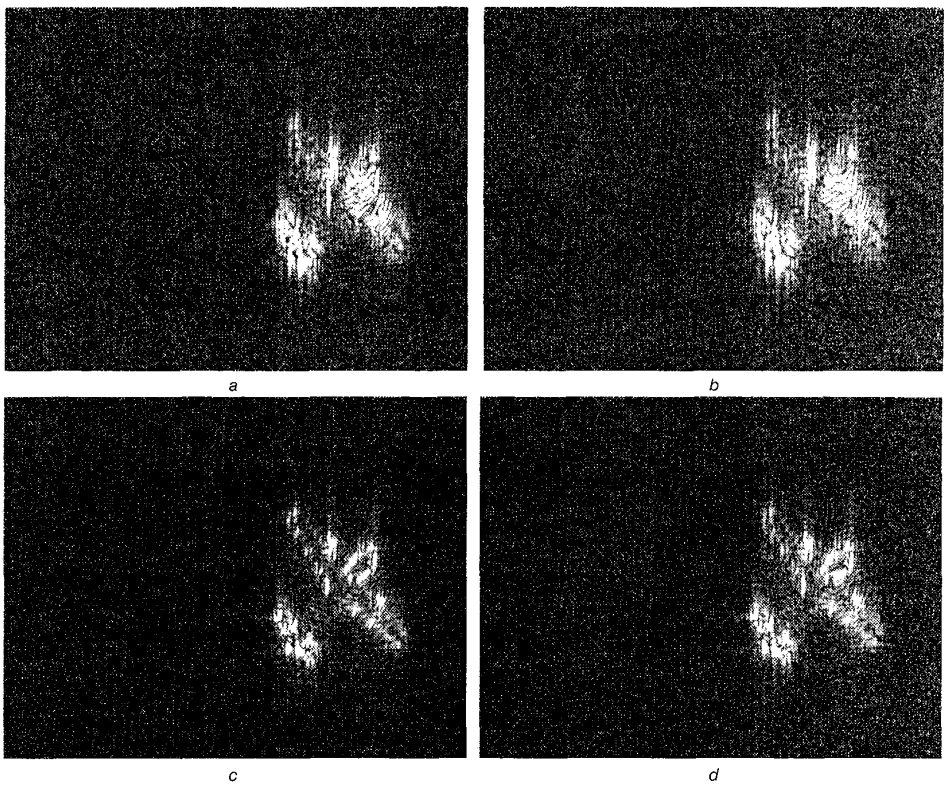

Fig. 5 *Processing of synthetic SAR image of aeroplane*

a Synthetic SAR image degraded by quadratic phase error and SαS clutter with $\alpha = 1.75$ and SCR = 0 dB
b SAR image focused using second-order phase difference (PD) method
c SAR image focused using PD-FLOS method with $p_1 = p_2 = 0.2$
d SAR image focused using PD-FLOS method with $p_1 = p_2 = 0$

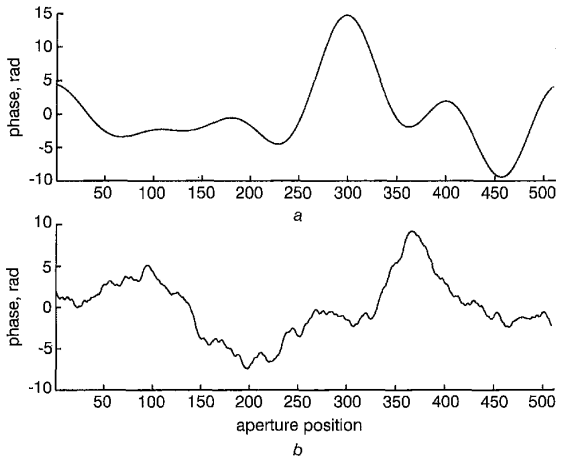

Fig. 6 *Phase errors*

a Tenth-order polynomial phase error used to produce the image shown in Fig. 7*b*
b Power law phase error used to produce the image shown in Fig. 8*b*

Sandia National Laboratories in New Mexico, USA. We used the two controlled phase error functions shown in Fig. 6 to defocus the images. We implemented the full PGA structure in Fig. 3 using the two PGA adjacent-pulse kernels described by eqns. 17 and 19. The windowing step was implemented by reducing the window size by $\frac{1}{3}$ at each iteration. Three iterations of the algorithms were employed.

The first test image, shown in Fig. 7*a*, depicts a rural scene with no apparent man-made targets. A road cutting the scene diagonally with trees on either side and a field on the upper part are the only features present in the image. Obviously, this is a highly clutter-like scene. First, the image was corrupted by the tenth-order polynomial phase error function, shown in Fig. 6*a*. The RMS value of the applied phase error is 5.31 rad. The resulting defocused image is shown in Fig. 7*b*. Figs. 7*c* and *d* show the results after three iterations of corrections by means of the two-pulse PGA-MLG and PGA-FLOS ($p_1 = p_2 = 0.2$) algorithms, respectively. The resulting RMS error associated with PGA-LMG is 0.89 rad, while the RMS error corresponding to PGA-FLOS is 0.58 rads (the error is 0.63 rad when $p_1 = p_2 = 0$). The RMS errors and the visual comparison of the focused results indicate that for this clutter-

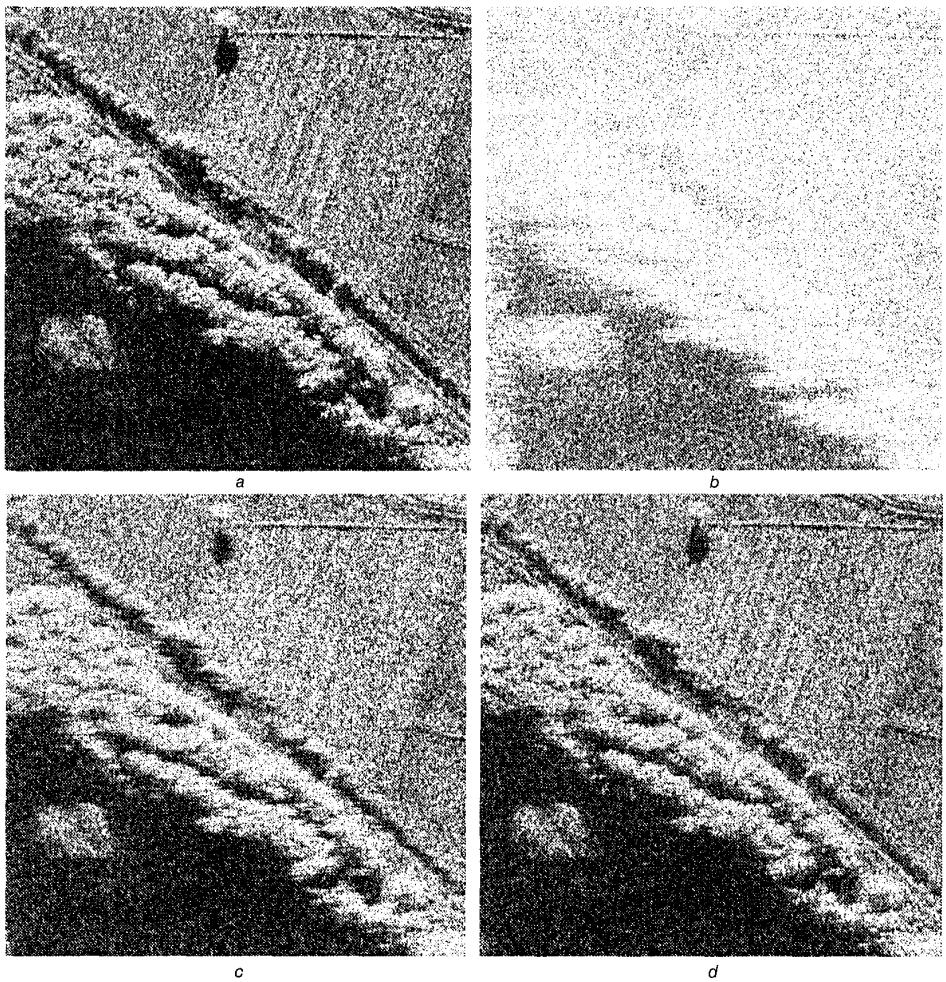

Fig. 7 *Processing of SAR image of rural scene*

a Original SAR image of rural scene
b SAR image degraded by tenth-order polynomial phase error
c Corrected using PGA-MLG
d Corrected using PGA-FLOS with $p_1 = p_2 = 0.2$

limited image, PGA-FLOS produces a superior focus quality. Notice that the foliage beneath the road in Fig. 7*d* appears to be nearly restored to the correct focus by PGA-FLOS.

Fig. 8 depicts the second test image, which is an urban scene having a dense set of large cross-section targets with intermingled tree shadows. This image is corrupted by the power law, high-order phase error function, shown in Fig. 6*b*, which is rich in high spatial frequency content [7]. The RMS value of the applied phase error is 3.62 rad. The resulting defocused image is shown in Fig. 8*b*. Figs. 8*c* and *d* show the results after three iterations of the PGA-MLG and PGA-FLOS ($p_1 = p_2 = 0.2$) algorithms, respectively. The resulting rms error associated with PGA-LMG is 0.28 rad, while the RMS error corresponding to PGA-FLOS is 0.25 rad (the error is 0.32 rad when $p_1 = p_2 = 0$). In this example, the existence of large magnitude dominant scatterers in the original image helps both methods achieve comparable focusing results. The RMS values still favour the PGA-FLOS method that uses $p_1 = p_2 = 0.2$, but the visual comparison of Figs. 8*c* and *d* suggests that notable performance improvement should not be expected from PGA-FLOS when focusing high signal-to-clutter ratio scenes.

5 Conclusions

Radar engineers have recognised the fact that effective clutter suppression is essential for target parameter estimation, detection and classification. In this paper, we have addressed the important problem of heavy-tailed clutter modelling and mitigation. We have presented a statistical model to characterise impulsive clutter by means of alpha-stable distributions. We then introduced a clutter-suppression tool based on fractional lower-order statistics and we used this tool in SAR autofocusing applications. Our proposed methods perform a nonlinear transformation of the measurements and they include the conventional algorithms as special cases. Thus, they provide flexibility that can be useful for optimisation purposes when operating in the presence of changing clutter/noise backgrounds.

Our future research in this area focuses on the derivation of a general maximum-likelihood phase error estimator, which will employ all available M pulses and will be based on alpha-stable modelling of the clutter in the measurements. The algorithm will then be compared to the general version of the eigenvector method by Jakowatz and Wahl, in real SAR imagery. Ideally, modelling the source of the phase errors, i.e. the platform motions, and combining the

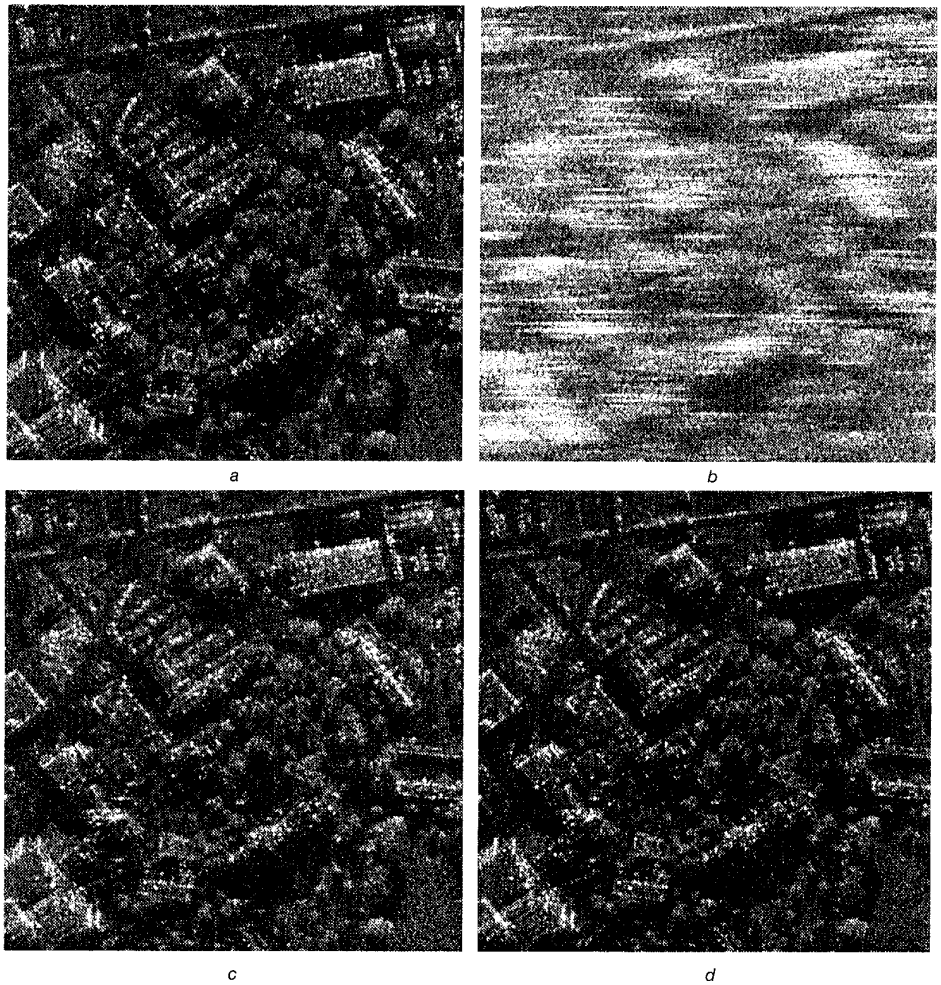

Fig. 8 *Processing of SAR image of urban scene*
a Original SAR image of urban scene
b SAR image degraded by power law phase error
c Corrected using PGA-MLG
d Corrected using PGA-FLOS with $p_1 = p_2 = 0.2$

resulting information with noise suppression processing could lead to improved phase estimates and robust autofocusing algorithms. This is another avenue of research that we are currently pursuing.

6 Acknowledgments

The work in this paper was supported by the Office of Naval Research under Contract N62269-96-C-0078. The first author was also supported by the Greek General Secretariat for Research and Technology under Program EIIET II, Code 97EA-152. The authors would like to thank Dr. Daniel Wahl from Sandia National Laboratories, who provided the real SAR imagery data.

7 References

1 RICHARDS, M.A.: 'Motion compensation fundamentals', *in* SCHEER, J.A., and KURTZ, J.L. (Eds.): 'Coherent radar performance estimation' (Artech House, Boston, 1993), pp. 101–112
2 CARRARA, W.G., GOODMAN, R.S., and MAJEWSKI, R.M. (Eds.): 'Spotlight synthetic aperture radar: signal processing algorithms' (Artech House, Boston, 1995)
3 BROWN, W.D., and GHIGLIA, D.C.: 'Some methods for reducing propagation-induced phase errors in coherent imaging systems. I. Formalism', *J. Opt. Soc. Am. A, Opt. Image Sci.*, 1988, **5**, pp. 924–942
4 MANCILL, C.E., and SWIGER, J.M.: 'A map drift autofocus technique for correcting higher order SAR phase errors (u)'. Twenty-Seventh Annual Tri-Service Radar Symposium Record, June 1981, Monterey, CA, pp. 391–400
5 YOJI, G.N.: 'Phase difference auto focusing for synthetic aperture radar phase correction'. United States Patent 4,999,635, March 1991
6 EICHEL, P.H., GHIGLIA, D.C., and JAKOWATZ, C.V.: 'Speckle processing method for synthetic aperture radar phase correction', *Opt. Lett.*, 1989, **14**, pp. 1–3
7 JAKOWATZ, C.V, and WAHL, D.E.: 'Eigenvector method for maximum-likelihood estimation of phase errors in synthetic-aperture radar imagery', *J. Opt. Soc. Am. A, Opt. Image Sci.*, 1993, **10**, pp. 2539–2546
8 WAHL, D.E., EICHEL, P.H., GHIGLIA, D.C., and JAKOWATZ, C.V.: 'Phase gradient autofocus—a robust tool for high resolution SAR phase correction', *IEEE Trans. Aerosp. Electron. Syst.*, 1994, **30**, pp. 827–834
9 NIKIAS, C.L., and SHAO, M.: 'Signal processing with alpha-stable distributions and applications' (John Wiley and Sons, New York, 1995)
10 TSAKALIDES, P., and NIKIAS, C.L.: 'Maximum likelihood localization of sources in noise modeled as a stable process', *IEEE Trans. Signal Process.*, 1995, **43**, pp. 2700–2713
11 SEKINE, M., OHTANI, S., MUSHA, T., IRABU, T., KIUCHI, E., and HAGISAWA, T.: 'Weibull distributed ground clutter', *IEEE Trans. Aerosp. Electron. Syst.*, 1981, **17**, pp. 596–598
12 RAGHAVAN, R.S.: 'A method for estimating parameters of K-distributed clutter', *IEEE Trans. Aerosp. Electron. Syst.*, 1991, **27**, pp. 238–246
13 ANASTASSOPOULOS, V., LAMPROPOULOS, G.A., DROSOPOULOS, A., and REY, M.: 'High resolution radar clutter statistics', *IEEE Trans. Aerosp. Electron. Syst.*, 1999, **35**, pp. 43–60
14 TSAKALIDES, P., RASPANTI, R., and NIKIAS, C.L.: 'Angle/Doppler estimation in heavy-tailed clutter backgrounds', *IEEE Trans. Aerosp. Electron. Syst.*, 1999, **35**, pp. 419–436
15 TSAKALIDES, P., and NIKIAS, C.L.: 'Robust space-time adaptive processing (STAP) in non-Gaussian clutter environments', *IEE Proc., Radar Sonar Navig.*, 1999, **146**, pp. 84–94
16 NOLAN, J.P.: 'Numerical calculation of stable densities and distribution functions', *Commun. Stat.-Stoch. Models*, 1997, **13**, pp. 759–774
17 CAMBANIS, S.: 'Complex symmetric stable variables and processes', *in* SEN, P. (Ed.): 'Contributions to statistics: essays in honor of Norman L. Johnson' (North-Holland, New York, 1983), pp. 63–79
18 TSAKALIDES, P., and NIKIAS, C.L.: 'The robust covariation-based MUSIC (ROC-MUSIC) algorithm for bearing estimation in impulsive noise environments', *IEEE Trans. Signal Process.*, 1996, **44**, pp. 1623–1633
19 MA, X., and NIKIAS, C.L.: 'Joint estimation of time delay and frequency delay in impulsive noise using fractional lower-order statistics', *IEEE Trans. Signal Process.*, 1996, **44**, pp. 2669–2687